

# Atomic Force Microscopy and High Resolution Scanning Electron Microscopy Investigation of Zeolite A Crystal Growth. Part 2: In Presence of Organic Additives.

*Pablo Cubillas,<sup>\*,†</sup> James T. Gebbie,<sup>†</sup> Sam M. Stevens,<sup>†</sup> Nicola Blake,<sup>†</sup> Ayako Umemura,<sup>†</sup>*

*Osamu Terasaki<sup>‡</sup> and Michael W. Anderson<sup>†</sup>*

<sup>†</sup>Centre for Nanoporous Materials. School of Chemistry. The University of Manchester. Oxford Road.  
Manchester. M13 9PL. UK.

<sup>‡</sup>Department of Physical, Inorganic and Structural Chemistry, Stockholm University, 10691 Stockholm,  
Sweden.

\* Corresponding author: Department of Earth Sciences, Durham University, Science Labs, DH1 3LE,  
Durham, UK. e-mail: [pablo.cubillas@durham.ac.uk](mailto:pablo.cubillas@durham.ac.uk). Tel: +441913341710

## **Abstract**

The nanoscopic details of the crystal growth of zeolite A in the presence of the organic modifiers diethanolamine (DEA) and triethanolamine (TEA) has been determined using a combination of atomic force microscopy (AFM) and high-resolution scanning electron microscopy (HRSEM) coupled with Monte Carlo simulations. Crystallization of zeolite A in the presence of TEA was faster than when the growing solution contained DEA. In addition the morphology of the final zeolite A crystals depended on the type of organic molecule, with TEA producing crystals bound only by {100} facets and DEA leading to the formation of relatively large {110} faces. These features can be explained in terms of the relative Si/Al in the growing medium and its control due to the different affinity of the organic molecules to Al. In addition, synthesis performed at 90 °C showed the appearance of {211} facets. Careful review of the HRSEM and AFM images, in addition to comparison with the MC simulations reveal that these are in fact pseudo-facets, product of the slow dissolution of the metastable zeolite A crystals. This

proves that the final habit of the LTA crystals can be governed by very small changes of saturation of the growing medium and a control of this parameter can prove advantageous when designing crystals for industrial applications.

*KEYWORDS: microporous materials, crystallization, scanning probe microscopy, electron microscopy.*

## 1. INTRODUCTION

The role of organic additives in the synthesis of zeolite A has received considerable attention in the past.<sup>1-7</sup> The most widely used additive is triethanolamine (TEA), which has been used to produce large zeolite A crystals.<sup>5, 6</sup> This is because TEA complexes with  $Al^{3+}$  ions through its hydroxyl groups, and then it releases them slowly, reducing the rate of nucleation.<sup>2</sup> Other tertiary alkanolamines have shown a similar behaviour.<sup>1</sup> Petranovskii et al.<sup>7</sup> investigated the effect of TEA in addition to triisopropanolamine, diisopropanolamine and diethanolamine (DEA). They found that crystals formed in the presence of secondary amines showed the formation of large {110} faces. This was in contrast to the morphology of those crystals grown with tertiary amines which were bound exclusively by {100} faces. Petranovskii et al. attributed the change in morphology to the formation of a new aluminium complex in the presence of the secondary amines, as shown by NMR spectroscopy<sup>7</sup>. In spite of these studies, no detailed nanoscopic analysis of the crystal growth of zeolite A in the presence of additives exists in the literature. In a previous paper<sup>8</sup> we demonstrated the usefulness of atomic force and high resolution scanning electron microscopy (AFM and HRSEM) for unravelling the full picture of zeolite A crystal growth, from nucleation to the end of synthesis, in an organic-free system. In this paper we have followed a similar approach to study the synthesis of zeolite A in the presence of two organic additives: triethanolamine and diethanolamine. Additionally, we have performed Monte Carlo simulations to further understand the growth features observed at near-equilibrium conditions on all crystal faces.

## 2. EXPERIMENTAL SECTION

**2.1 Synthesis.** Synthesis of zeolite A in the presence of TEA, DEA and a 50%-50% TEA-DEA mixture was carried out following the procedure developed by Petranovskii,<sup>7</sup> which is, in turn, derived

from the original method of Charnell to grow large zeolite A and zeolite X crystals.<sup>5</sup> The molar composition of the solutions used was:  $0.86\text{Na}_2\text{O}:0.44\text{SiO}_2:0.42\text{Al}_2\text{O}_3:5.71\text{R-OH}:111\text{H}_2\text{O}$ . The concentration of DEA/TEA was adjusted to achieve a constant molar ratio of 5.71 R-OH groups per synthesis. A solution of sodium metasilicate was prepared by dissolving the corresponding amount of sodium metasilicate pentahydrate (Fluka, purum >97%) in one half of the total water. To this solution one half of the corresponding DEA (BDH) or TEA (Aldrich) was added. The aluminate solution was prepared by mixing the required amount of sodium aluminate (FSA, anhydrous) to the remaining water. The second half of TEA/DEA was added to this solution. The two solutions were mixed and stirred for a few minutes before being divided into several polypropylene bottles and introduced in ovens at the required temperature. Two different batches of experiments were carried out. In the first batch, experiments were carried out at two different temperatures (75 and 90 °C), three experimental times (10, 14 and 20 days) and for three different contents of DEA/TEA, as shown in Table 1. The second batch was carried out exclusively in the presence of diethanolamine and is summarized in Table 2. Once a specified synthesis time was completed the corresponding polypropylene bottle was extracted from the oven and immediately introduced in a bath of cold water. This “quenching” step decreased the solution temperature (and the rates of any growth/dissolution reactions) very rapidly minimising any possible changes in the surface topology. The synthesis product was then washed in deionized water until the pH was below 9, filtered, and left to dry overnight at 80 °C. This treatment was not expected to produce any modifications on the zeolite A surface topography either as it has been shown that dissolution of this phase only takes place at very high pH (above 13) at a significant rate (to modify the surface features in a few hours).<sup>9</sup>

**2.2 Scanning Electron Microscopy.** SEM images were obtained using a FEI Quanta environmental scanning electron microscope. Samples were prepared by spreading zeolite powder on a carbon tape stuck on a metal stub followed by sputter coating with gold to reduce charging effects under the electron beam. For acquiring high-resolution SEM images, samples were placed on a conductive surface but left

uncoated and were taken using a JEOL JSM-7401F (cold-FESEM) using the Everhart–Thornley secondary electron detector.

**Table 1.** Samples prepared to compare different organic additives in the synthesis of zeolite A

Temperature (°C)	100% TEA	100% DEA	50%/50% TEA/DEA	Time (days)
75	S1	S5	S9	10
75	S2	S6	S10	14
75	S3	S7	S11	20
90	S4	S8	S12	10

**Table 2.** Samples prepared to compare different temperatures and times in the synthesis of zeolite A

60°C		75°C		90°C	
Time (days)	code	Time (days)	code	Time (days)	code
2	S13	2	S19	2	S25
4	S14	3	S20	3	S26
6	S15	4	S21	4	S27
8	S16	5	S22	5	S28
12	S17	7	S23	7	S29
14	S18	10	S24	10	S30

**2.3 Atomic Force Microscopy.** AFM images were acquired using a JPK instruments Nano Wizard II. Images were taken on contact mode. Standard silicon nitride tips (NP Bruker Probes), with a nominal radius of 20 nm and a nominal spring constant of 0.58 N/m were used.

**2.4 Powder X-ray diffraction.** Powder X-ray diffraction patterns were obtained by means of a Philips X’pert diffractometer using Cu–K $\alpha$  radiation.

**2.5 Monte Carlo simulations.** Monte Carlo simulations were performed using an in-house Fortran 90 program with graphics rendered in an in-house program constructed in C++ utilising the

OpenGL application programming interface. In order to investigate the crystal growth of zeolite A, a highly simplified model was constructed in order to draw out the most important aspects that control crystal habit. The simplification is based upon our knowledge that closed-cage structures in zeolites are substantially more stable than open-cage structures<sup>10</sup>. This comes from a careful analysis of the AFM aided dissolution of zeolite L whereby the structure was “unstitched” unit-by-unit. This dissolution occurred in a set of seven discrete steps all of which involved closed-cage structures indicating that these are by far and away the most stable entities and therefore the rate-determining structures. In zeolite A there are three closed-cage structures: the double four ring (D4R), the BETA ( $\beta$ ) cage and the ALPHA ( $\alpha$ ) cage. These cages fill space to form the zeolite A framework. If a given cage is closed, that cage is complete in terms of all tetrahedral silicon or aluminium atoms being present. Then every tetrahedral site (T-site) is of  $Q_3$  connectivity at the surface of the crystal. If a given cage is incomplete then T-sites at the surface can be of  $Q_1$  or  $Q_2$  connectivity, making the energy of the open-cage substantially higher and more unstable. Therefore, in terms of the kinetics of crystal growth the formation of stable closed-cage structures will be rate determining. As a consequence the simulation can be coarse grained into the growth of whole closed-cages – even though in reality the fundamental growth mechanism will be by smaller oligomers. By adopting this approach it is not important the nature of the growth units because the kinetics are controlled overwhelmingly by the relative stability of the more stable surface structures. This, in effect, allows us to concentrate on the crystalline phase rather than the solution phase. In this simplified model there are only four unknown energy values that need to be determined. These are the energy penalties for T-O-T condensation in each of the three cage types  $U_{D4R}$ ,  $U_{\beta}$  and  $U_{\alpha}$  (given as  $U_i$  in the equations below) plus the driving force energy  $\Delta\mu$  (related to the supersaturation). Supersaturation is notoriously difficult to measure in zeolite syntheses but, for our purposes, we focus on a well-defined driving force,  $\Delta\mu$ , without trying to make the precise link between  $\Delta\mu$  and supersaturation. This is a pragmatic approach but still quite powerful as we are able to determine the consequences of increasing

or decreasing driving force which, for the experimentalist, means increasing or decreasing supersaturation respectively. The program is able to determine the value of  $\Delta\mu_{\text{eq}}$  at the equilibrium point by decreasing  $\Delta\mu$  for a growth event and increasing  $\Delta\mu$  for a dissolution event. In this manner the dynamic equilibrium is approached. As a consequence it is possible to run the program in conditions of either super-saturation or under-saturation by choosing values of  $\Delta\mu$  above or below  $\Delta\mu_{\text{eq}}$ . Also, as the program determines the value of the driving force energy at equilibrium the  $\Delta\mu$  term becomes known when equilibrium is reached reducing the unknown parameters to three if comparisons are made with crystals withdrawn at the end of the synthesis close to equilibrium. To understand the energetic considerations made in this simplified approach a number of hypothetical cases can be considered. The  $\beta$  cage consists of 24 T-sites, two hypothetical extremes can be considered. The first is a  $\beta$  cage that is within the crystal bulk, all 24 T-sites will be present and exhibit  $Q_4$  connectivity. This first extreme case represents the most stable configuration a closed-cage can take, every other configuration can be considered to be energetically destabilised with respect to this configuration. The second case would be the formation of a closed  $\beta$  cage from all 24 T-sites (all are  $Q_3$  connectivity), this would represent the most energetically destabilised case with respect to the crystal bulk. Every growth site at the crystal surface will fall between these two extremes, where the energy required for formation of a given closed-cage is proportional to the number  $n$  of  $Q_3$  T-sites in the closed cage. Thus if the energy penalty of transforming a  $Q_3$  to a  $Q_4$  site in the  $\beta$  cage is  $U_\beta$  then the energy required to form the closed cage is proportional to  $n$ . The same logic can then be applied to the energetics of the remaining two cage types to yield an energetic model in which the energy penalty parameters can be assigned various quantities and their effect upon crystal habit observed. Probabilities for growth relative to dissolution were calculated according to the protocol of Boerrigter et al.<sup>11</sup> using an approach similar to that described by Brent et al.<sup>10</sup> recently for zeolite L. Considering a specific site for growth ( $T_n$  where  $T$  is  $\alpha$ ,  $\beta$  or D4R and  $n$  the number of  $Q_3$  sites

in the cage to be grown or dissolved) then the relative probability for growth,  $P_G^{T_n}$ , and dissolution,  $P_D^{T_n}$ , is:

$$P_G^{T_n} = \exp\left(\frac{-0.5nU_i}{kT} + \frac{0.5\Delta\mu}{kT}\right)$$

$$P_D^{T_n} = \exp\left(\frac{0.5nU_i}{kT} - \frac{0.5\Delta\mu}{kT}\right)$$

The terms 0.5 in the above equation arise from a symmetry between growth and dissolution. This may not be strictly correct but we have no experimental evidence to suggest the contrary. Indeed all measurements that we have made on nanoporous systems previously by in situ AFM where it is possible to adjust conditions repeatedly above and below saturation suggest that growth and dissolution is, more-or-less, symmetric.

### 3 RESULTS

**3.1 Effect of temperature and alcohol** Figure 1 shows a series of SEM micrographs of the zeolite A crystals obtained from the first batch of experiments, performed in the presence of TEA and DEA (images of the crystals from synthesis containing DEA-TEA mixtures are shown on Figure S1 in the supplementary information). It can be seen in the images that there is a clear change in morphology depending on the type of organic additive. Those crystals synthesised in the presence of DEA are bound by {100} and {110} faces, whereas those synthesised with TEA only and with the DEA-TEA mixture are bound by {100} facets only. Figure 1a show the presence of amorphous gel particles indicating that after 10 days the crystal growth is not completed for those experiments performed with TEA. The same situation is repeated for the DEA-TEA experiments (Figure S1a). This situation is more clearly illustrat-

ed in Figure 2 which shows a graph of the maximum crystal size as a function of synthesis time for all experiments of batch 1.

It can also be seen that the crystals synthesised in the presence of DEA have reached their maximum size by 10 days, indicating that the reaction proceeds faster in the presence of DEA. Additionally, the crystal size increases with the content of DEA as well as with an increase in temperature. These results confirm some of the findings from Petranovskii.<sup>7</sup> The presence of DEA also had an effect on the type of phases precipitating by completely inhibiting the formation of zeolite X which was always present in those syntheses containing TEA. The formation of LOSOD was observed in all experiments in various proportions (never more than 10%).

Another significant observation for this batch of samples was the presence of a new face. This can be seen clearly in Figure 1f showing a zeolite A crystal grown in the presence of DEA at 90 °C for 10 days. The additional facets along the edges of the crystal are parallel to the {211} planes. This kind of facets have not been reported previously for this system, but are significant as they represent a lessening of the sharpness of the edges of the crystals. This is a preferred property for applications as detergent builders.

In addition to studying the effects on morphology by means of SEM, the surface topography of the various samples was studied by AFM. Figure 3 shows results from these observations for most of the samples of the batch 1 synthesised in the presence of TEA and DEA (images from the experiments performed with DEA-TEA mixtures are shown in Figure S1d-g). Figures 3a and 1Sd show the presence of multiple 2-D nuclei on the {100} surface of zeolite A crystals extracted after 10 days and grown in the presence of pure TEA and the 50-50 mixture (at 75°C). This corroborates the fact that the crystals were still under at least medium-supersaturation conditions, i.e. the crystal growth had not reached equilibrium. In comparison the image taken at 10 days on the pure DEA synthesis (Figure 3e) shows a birth-and-spread growth mechanism with much lower nucleation density, indicative of close-to-equilibrium condi-

tions,<sup>8</sup> as expected from trends seen in Figure 2. Images taken at 20 days in samples synthesised at 75 °C show invariably the operation of a low density birth-and-spread growth mechanism indicating, as expected at this point of the synthesis, close-to-equilibrium conditions. It can also be observed that the corners of the terraces are, in all cases, rounded, to the point of producing almost circular terraces for those of small sizes. Finally, AFM observations on crystals synthesised at 90 °C for 10 days reveal a more contrasting surface topography. For those crystals synthesised in the presence of pure TEA terrace corners become more rounded (Figures 3c and d), but in the crystals grown with the DEA/TEA mixture and DEA terraces adopt a quasi-diamond shape, with edges running approximately parallel to the  $\langle 110 \rangle$  directions (Figures 3g and 1Sf). This topography is also observed on terraces on the  $\{110\}$  face of crystals synthesised with DEA only (Figure 3h).

**3.2 Effect of time and temperature on DEA-only synthesis.** In light of results from the batch 1 experiments a new series of syntheses were conducted with pure DEA to study the effect of temperature and time (Table 2). Results from these experiments show that the crystal growth rate increases as a function of temperature, as expected. Crystal size analysis also reveals that the reaction is complete, i.e. that no further increase in crystal size is taking place, after 8, 4 and 2 days for experiments performed at 60, 75 and 90 °C, respectively. All crystals produced in these syntheses show  $\{100\}$  and  $\{110\}$  faces, see Figure 4. The relative size of these faces change as a function of temperature, with crystals synthesised at higher temperatures (90 °C) exhibiting relatively smaller  $\{110\}$  faces. Interestingly, the relative size of the  $\{110\}$  faces also depends on the crystal size, as can be seen in all three images, where the smaller crystals show the smaller  $\{110\}$  facets.

AFM images of crystals from the second batch of experiments are shown in Figure 5. Figures 5a and 5b show images of the  $\{100\}$  face of crystals at the end of their synthesis (14 and 10 days), and grown at 60 and 75 °C, respectively. In both cases, it can be seen that the prevailing growth mechanism at those times was of birth and spread, indicating close-to-equilibrium conditions. Additionally the ter-

race corners are sharp. In contrast images taken on crystals grown at 90 °C show rounded terraces (Figures 5c and 5d) after 2 and 10 days of synthesis. Analysis of the radius of curvature of these rounded corners reveals an increase with the time of the reaction, as can be seen by comparing Figures 5c and 5d.

High-resolution SEM observations near the apex of crystals synthesised at 90 °C show the appearance of {211} facets after 2 days of synthesis (Figure S2 in supplementary information). The size of the facet increases with time, as can be seen by comparing Figures S2a and S2b which show images of crystals after 2 and 7 days of synthesis respectively. Figure S2c shows an AFM image of these {211} facets that do not exhibit any clear steps or terraces.

#### 4. DISCUSSION

The formation of the {110} face on zeolite A crystals has been observed in syntheses in both the absence and in the presence of organic molecules.<sup>6-8, 12-14</sup> In syntheses performed in the absence of organic compounds, its appearance has been related to a decrease in the Si/Al ratio,<sup>12</sup> although it has been shown recently that a more complex relationship to the overall gel/solution composition dictates its formation.<sup>13, 14</sup>

In synthesis where organic molecules are present additional organic-surface interactions may influence the formation of a particular face, but in the case of TEA, it has been found that the molecule is not included in the pore space of the final zeolite A products, indicating a lack of strong interaction between organic and framework. In the case of DEA there is no data available in the literature regarding its inclusion in the zeolite A pore space<sup>4</sup>, for that reason we performed C-NMR on some of the synthesised crystals. Results from these analyses indicated the absence of DEA molecules within the zeolite A pores. Therefore, the influence of DEA vs. TEA on the presence of {110} face can be explained according to the differences in the binding of Al by the two molecules and its effect on the Si/Al ratio in the growing solution..

Results from Petranovskii et al.<sup>7</sup> show that, in the presence of TEA, Al binds completely to the organic, resulting in the formation of a chelate. This has the effect of decreasing substantially the amount of Al(OH)<sub>3</sub> available for nucleation and crystal growth of the zeolite. In fact, Al concentration will be completely controlled by the rate of release from the TEA-chelate. On the contrary, DEA was found to bind less well to Al, decreasing the Al(OH)<sub>3</sub> concentration only marginally.<sup>77</sup> In light of these results it can be argued that, in the case of the experiments performed with DEA only, the amount of “free” Al available for crystal growth would be much higher than in the case of those performed with TEA, i.e., TEA experiments will have a higher Si/Al ratio and therefore a more cubic morphology could be expected. The stronger Al-binding strength and slower release rate of the TEA molecules also explain why the synthesis proceeds faster in the presence of DEA.

With the goal of further understanding the role of organic molecules on controlling the LTA morphology we performed tens of thousands of simulations of micron-sized crystals varying the three energy penalties for D4R, BETA and ALPHA cages and from these we noted a number of trends. The first, important trend was that the absolute value of the energy penalty did not have much influence on the crystal habit. The habit was controlled more by the relative ratio of the energy penalties of the different cages. The absolute value has a strong influence on the terrace density at a given driving force. Therefore, in terms of crystal habit alone we are able to formulate a triangular plot of crystal habit versus relative concentration of the three energy penalties for the three cage types and this is shown in Figure 6. The phase space is dominated by cubic morphology and indeed that shape prevails at the centre of stability where the energy penalty for the three cage types is identical. Other substantial regions present predominantly either spherical or rhombic dodecahedral morphology, but it is important to highlight their relative smaller size in terms of the total area of the triangle, which is in agreement with experimental observations in multiple zeolite A synthesis routes, where the {100} is always present<sup>6, 7, 12, 15, 16</sup>. Furthermore, the shape of the transition zone indicates that small variations in the stability of the ALPHA

cage can have a potential large effect in the morphology of the crystals. In the transition zones the crystals show more than one facet, including the {111} face, in some cases. Therefore, the morphology produced by the classic inorganic synthesis route will fall in this area<sup>8</sup>. In addition, crystals from our experiments with DEA lie in the transition zone between cubes and rhombic dodecahedra exhibiting primarily {100} and {110} facets.

It is also reasonable to assume that the energy penalties for the three cage types will not be too far removed from the centre of stability, i.e. we would expect the stability of each type of cage to be similar. On this basis the simulations performed at positions 1 and 2 on Figure 6 are presented in Figure 7. The relative energy penalties D4R:BETA:ALPHA for the three cage types in this simulation at points 1 and 2 were 0.36:0.36:0.28 and 0.42:0.42:0.16 respectively. Absolute values of the energy penalties at point 2 that resulted in correct simulation of the terrace nucleation density were 2.5 kcal/mol, 2.5 kcal/mol and 1.5 kcal/mol. The equilibrium morphologies obtained from the simulation (Figures 7b and 7e) show a considerable agreement with the shapes of the crystals synthesised in this study. This fact leads to a few important additional observations. The first is that, the simulations corroborate the experimental result that shows that small changes in solution chemistry, from 100 % DEA to 50-50 TEA-DEA, can lead to dramatic changes in crystal morphology. On the other hand if we compare the morphologies from crystals grown in 100% DEA to those grown in inorganic solutions, both are contained within the relative “thin” transition zone, which may indicate a “smaller” effect by the DEA on the relative cage stabilisation energies. This could be explained in terms of the smaller Al-binding “potential” of the DEA, when compared to TEA.

The simulations in Figure 7 show the power of this methodology for predicting crystal morphology in non-equilibrium situations, both super-saturated and under-saturated. This is not readily achieved by more conventional determinations of crystal morphology based on attachment energies or surface energy alone that normally determine the thermodynamic equilibrium structure alone.<sup>17, 18</sup> At supersatu-

rated conditions the crystals show a high surface nucleation density. At equilibrium the density of surface nucleation is diminished and the terraces coalesce and form geometric shapes consistent with the crystal symmetry. These results follow the same trends observed on our synthesis, for crystals extracted whilst still at supersaturation conditions (Figures 3a and S1d), as well as equilibrium (Figures 3b, 3e and 1Se). At undersaturated conditions both the crystal edges are dissolved revealing higher index facets and the surface terraces reform to reveal higher index edges. This later phenomenon directly aligns with the results for the synthesis with DEA under higher temperature conditions (90 °C) where {211} facets are created and the surface terraces on the {100} change from square to diamond shape and on {110} from rectangular to truncated rectangular. Therefore, the observed {211} facets are in fact pseudofacets created by very slow dissolution and not by a net growth progress. In fact, careful review of the HRSEM images for crystals synthesised at 90 °C shows the presence of dissolution features, in the shape of small triangular etch pits and corroded twin boundaries (Figures 8). These features become more obvious when compared to twin boundaries of crystals synthesized at lower temperatures, where no {211} are present, i.e. no dissolution has taken place (Figure 8b). The creation of conditions of under-saturation is probably the result of consecutive crystal transformations whereby the metastable LTA crystals are starting a process of re-dissolution and transformation into a lower energy phase such as hydroxysodalite.<sup>19</sup>

A further consequence of undersaturation is also shown in Figure 9 whereby crystal imperfections act to prevent crystal dissolution. This has the effect of pinning terrace retreat and the creation of protrusions at the crystal surface with edges parallel to [100]. This experiment in fact reveals the presence of these point defects which are only exposed upon dissolution and represent a new type of defect in the zeolite A system.

Another consequence of our calculations is that the simulation also determines the nature of the surface structure for a given ratio of cage stabilities and saturation condition, see Figure 10. Experimentally it is very difficult to determine the surface structure of a zeolite and the only method available is

high-resolution transmission electron microscopy. This has only been used in a limited number of instances owing to the extreme difficulty in the experimental protocol and the need for beam stable samples. Even then the technique only reveals a projection of the sample surface and further interpretation is still required.

In terms of closed-cage structures there are a small, finite number of surface terminations at equilibrium conditions, and these are shown in Figure 11. On the {100} facet there are four possible structures which are terminated by the BETA cage, the ALPHA cage and two by the double-four ring. Within the transition zone, shown by position 2 in Figure 6, the crystal develops both {100} and {110} facets, each showing a mixture of surface terminations. This is a result of a competition between two surface structures shown by a tick on Figure 11. For the {100} face the predominant surface structure is the double-four ring on top of the sodalite cage that is three times more abundant than the structure terminated by the BETA cage. It is not surprising that these two structures are in dynamic equilibrium at the surface of the crystal when the supersaturation is very low because the two surface structures present exactly the same surface density of  $Q_3$  groups. On the {110} surface there is a similar result in that there is a competition between two surface structures and the predominant termination is, again, the one displaying the larger amount of double four rings (Figure 11). This surface structure is three times more favourable than the same surface without the vertical double-four ring, which is terminated by a combination of ALPHA-cages and inclined double four rings (so only one of the 8 T sites at the ring is a  $Q_3$  site). As with the {100} surface this competition on the {110} surface is between two structures with exactly the same surface density of  $Q_3$  groups. It remains a challenge for experimental chemists to confirm which of these surface structural arrangements is actually displayed, or if indeed both are displayed. The results are, however consistent with previous in situ dissolution studies using AFM that showed that terraces on the (100) surface dissolved in a two-step process: first the double-four rings and then the BETA cages<sup>9,20</sup>.

## 5. CONCLUSIONS

Synthesis of zeolite A in the presence of TEA and DEA and a 50-50 mixture of TEA-DEA showed the formation of relatively large crystals (15-20  $\mu\text{m}$ ) with two distinct morphologies. Those crystals synthesised with pure TEA and the TEA-DEA mixture showed a perfect cubic morphology, whereas those grown in the presence of pure DEA were bound by  $\{100\}$  and large  $\{110\}$  facets. These results can be explained by looking at the Al-binding efficiency of the two different molecules. TEA is more effective in binding to Al, therefore limiting the amount of “free” Al in solution, on the contrary DEA has been found to be less effective. Therefore, those synthesis performed in DEA will have a smaller Si/Al which has been found to lead to the appearance of  $\{110\}$  facets in inorganic syntheses. In addition crystals synthesised at 90 °C in the presence of pure DEA showed the formation of  $\{211\}$  facets, which have not been described in the literature before. These facets are in fact pseudo-facets and the product of net-dissolution of the crystals due to the metastability of the zeolite A crystals at the end of the standard synthesis. Controlled formation of these facets could be potentially very useful for the detergent industry as it decreases the presence of sharp edges and corners in the crystals.

In addition, we performed Monte Carlo simulations to further understand the results. Thousands of simulations were performed by varying the degree of stability of the three closed-cage structures that compose the zeolite A structure (ALPHA, BETA and D4R). Simulations indicate that the final morphology is dictated by relative differences in the stabilities of the three cage-structures, and not on the absolute penalty energies. Results were displayed in a triangular diagram and show 4 distinct stability fields regarding final morphology: spherical, cubic, dodecahedral and a transition zone where the crystals display two ( $\{100\}$  and  $\{110\}$ ) and three ( $\{100\}$ ,  $\{110\}$  and  $\{111\}$ ) facets. Assuming that, in the real world, the cage stabilities will be similar we showed how small variations in the stability of the ALPHA

cage can lead to drastic differences in morphology. Therefore, potentially small variations in synthesis chemistry could result in large morphological variations, as our own results indicate and as the presence/absence of the {111} face in inorganic synthesis also indicate.

The power of our Monte Carlo method was illustrated by simulating zeolite A crystals under supersaturation and undersaturation conditions. Especially relevant where the simulations of crystals bound by {100} and {110} at undersaturated conditions, which showed the formation of circular terraces and {211} facets, confirming the experimental observations on the formation of the {211} pseudofacets. Finally simulations also provide a clue on the nature of the surface termination of the {100} and {110}, which tends to be dominated, by the least amount of Q<sub>3</sub> groups exposed.

## **ASSOCIATED CONTENT**

**Supporting Information:** Figure S1 containing SEM and AFM images of experiments performed with TEA-DEA mixture. Figure S2, containing HRSEM and AFM images of {211} evolution of size with experimental time. This material is available free of charge via the Internet at <http://pubs.acs.org>.

## **Author Contributions**

The manuscript was written through contributions of all authors. / All authors have given approval to the final version of the manuscript. / †‡ These authors contributed equally.

## **Funding Sources**

The work was supported by the EPSRC and ExxonMobil Research and Engineering.

## **ACKNOWLEDGMENTS**

The Authors would like to thank both EPSRC and ExxonMobil Research and Engineering for financial support.

## **REFERENCES**

1. Morris, M.; Dixon, A. G.; Sacco, A.; Thompson, R. W. Investigations on the Relative Effectiveness of Some Tertiary Alkanolamines in the Synthesis of Large-Crystal Zeolite NaA. *Zeolites* **1993**, *13* (2), 113-121.
2. Morris, M.; Sacco Jr, A.; Dixon, A. G.; Thompson, R. W. The Role of an Aluminum-Tertiary Alkanolamine Chelate in the Synthesis of Large Crystal Zeolite NaA. *Zeolites* **1991**, *11* (2), 178-183.
3. Schmitz, W.; Kornatowski, J.; Finger, G. Growth of NaA Zeolites in the Presence of Triethanolamine (Tea). The Influence of Water, TEA and Al Contents. *Cryst. Res. Technol.* **1987**, *22* (1), 35-41.
4. Scott, G.; Thompson, R. W.; Dixon, A. G.; Sacco, A. The Role of Triethanolamine in Zeolite Crystallization. *Zeolites* **1990**, *10* (1), 44-50.
5. Charnell, J. F. Gel Growth of Large Crystals of Sodium A and Sodium X Zeolites. *J. Cryst. Growth* **1971**, *8* (3), 291-294.
6. Yang, X. B.; Albrecht, D.; Caro, E. Revision of Charnell's Procedure towards the Synthesis of Large and Uniform Crystals of Zeolites A and X. *Microporous Mesoporous Mater.* **2006**, *90* (1-3), 53-61.
7. Petranovskii, V.; Kiyozumi, Y.; Kikuchi, N.; Hayamisu, H.; Sugi, Y.; Mizukami, F. The Influence of Mixed Organic Additives on the Zeolites A and X Crystal Growth. *Stud. Surf. Sci. Catal.* **1997**, *105A* (Progress in Zeolite and Microporous Materials, pt. A), 149-156.
8. Cubillas, P.; Stevens, S. M.; Blake, N.; Umemura, A.; Chong, C. B.; Terasaki, O.; Anderson, M. W. AFM and HRSEM Investigation of Zeolite A Crystal Growth. Part 1: In the Absence of Organic Additives. *J. Phys. Chem. C* **2011**, *115* (25), 12567-12574.
9. Meza, L. I.; Anderson, M. W.; Slater, B.; Agger, J. R. In Situ Atomic Force Microscopy of Zeolite A Dissolution. *PCCP* **2008**, *10* (33), 5066-5076.

10. Brent, R.; Cubillas, P.; Stevens, S. M.; Jelfs, K. E.; Umemura, A.; Gebbie, J. T.; Slater, B.; Terasaki, O.; Holden, M. A.; Anderson, M. W. Unstitching the Nanoscopic Mystery of Zeolite Crystal Formation. *J. Am. Chem. Soc.* **2010**, *132* (39), 13858-13868.
11. Boerrigter, S. X. M.; Josten, G. P. H.; de Streek, J. v.; Hollander, F. F. A.; Los, J.; Cuppen, H. M.; Bennema, P.; Meekes, H. Monty: Monte Carlo Crystal Growth on any Crystal Structure in any Crystallographic Orientation; Application to Fats. *J. Phys. Chem. A* **2004**, *108* (27), 5894-5902.
12. Thompson, R. W.; Huber, M. J. Analysis of the Growth of Molecular Sieve Zeolite NaA in a Batch Precipitation System. *J. Cryst. Growth* **1982**, *56* (3), 711-722.
13. Kosanovic, C.; Jelic, T. A.; Bronic, J.; Kralj, D.; Subotic, B. Chemically Controlled Particulate Properties of Zeolites: Towards the Face-Less Particles of Zeolite A. Part 1. Influence of the Batch Molar Ratio  $[\text{SiO}_2/\text{Al}_2\text{O}_3]_b$  on the Size and Shape of Zeolite A Crystals. *Microporous Mesoporous Mater.* **2011**, *137* (1-3), 72-82.
14. Bosnar, S.; Bronic, J.; Brlek, Đ.; Subotic, B. Chemically Controlled Particulate Properties of Zeolites: Towards the Face-Less Particles of Zeolite A. 2. Influence of Aluminosilicate Batch Concentration and Alkalinity of the Reaction Mixture (Hydrogel) on the Size and Shape of Zeolite A Crystals. *Microporous Mesoporous Mater.* **2011**, *142* (1), 389-397.
15. Grizzetti, R.; Artioli, G. Kinetics of Nucleation and Growth of Zeolite LTA from Clear Solution by in Situ and Ex Situ XRPD. *Microporous Mesoporous Mater.* **2002**, *54* (1-2), 105-112.
16. Zhu, G.; Qiu, S.; Yu, J.; Gao, F.; Xiao, F.; Xu, R.; Sakamoto, Y.; Terasaki, O. Synthesis of Zeolite LTA Single Crystals of Macro- to Nanometer Size, In: *Proceedings of the 12th International Zeolite Conference*, Baltimore, Maryland, U.S.A., Treacy, M. M. J.; Marcus, B. K.; Bisher, M. E.; Higgings, J. B., Eds. Materials Research Society, 1999; pp 1863-1870.
17. Hartman, P.; Bennema, P. The Attachment Energy as a Habit Controlling Factor: I. Theoretical Considerations. *J. Cryst. Growth* **1980**, *49* (1), 145-156.

18. Aquilano, D.; Rubbo, M.; Catti, M.; Pavese, A. Theoretical Equilibrium and Growth Morphology of CaCO<sub>3</sub> Polymorphs. I. Aragonite. *J. Cryst. Growth* **1997**, *182* (1–2), 168-184.
19. Tassopoulos, M.; Thompson, R. W. Transformation Behavior of Zeolite-A to Hydroxysodalite in Batch and Semibatch Crystallizers. *Zeolites* **1987**, *7* (3), 243-248.
20. Meza, L. I.; Anderson, M. W.; Agger, J. R. Differentiating Fundamental Structural Units During the Dissolution of Zeolite A. *Chem. Commun.* **2007**, (24), 2473-2475.

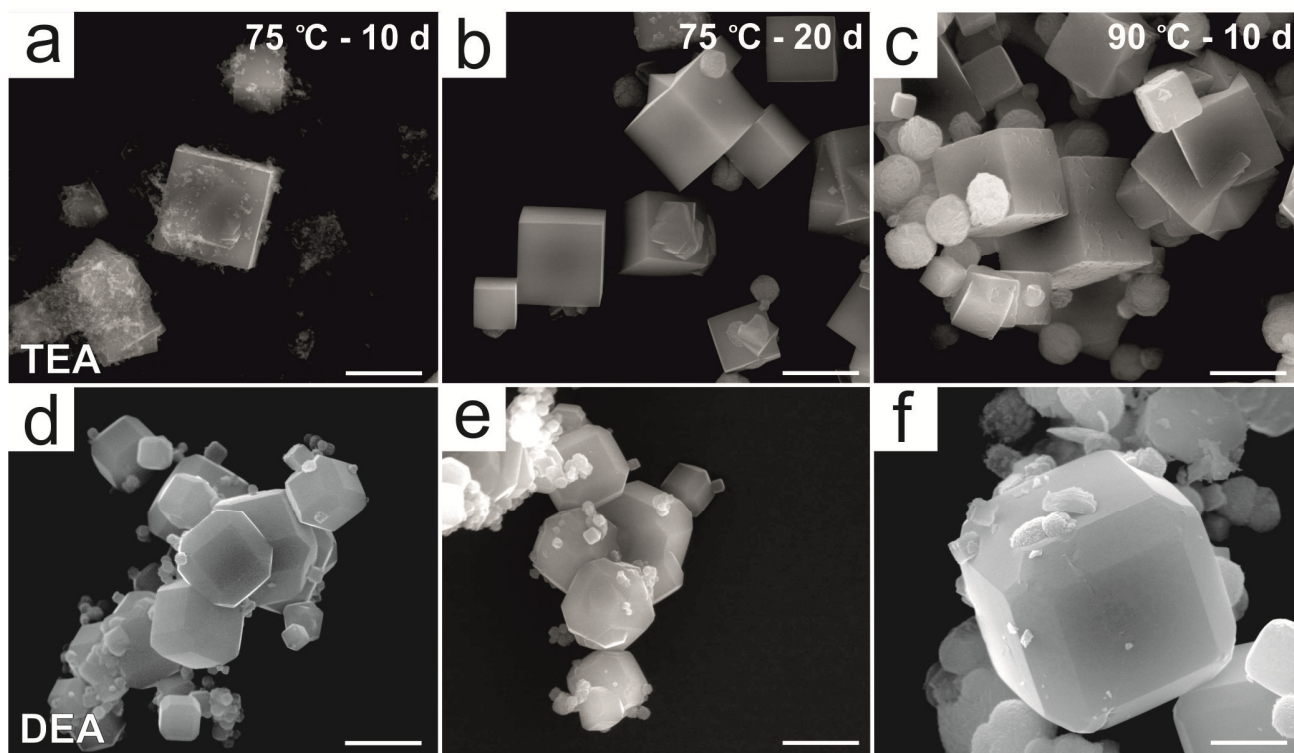


**Figure 1.** SEM micrographs from the first batch of experiments. a-c) Experiments performed with TEA at 75 °C-10 days (a), 75 °C- 20 days (b) and 90 °C – 10 days (c). d-f) Experiments performed with DEA at 75 °C-10 days (d), 75 °C- 20 days (e) and 90 °C – 10 days (f). Scale bars: a, b, c, d, e = 10  $\mu\text{m}$ ; f = 5  $\mu\text{m}$ .

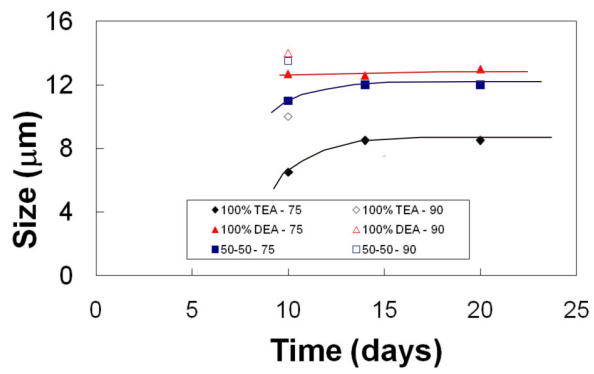


**Figure 2.** Evolution of size as a function of time for all experiments in batch 1.

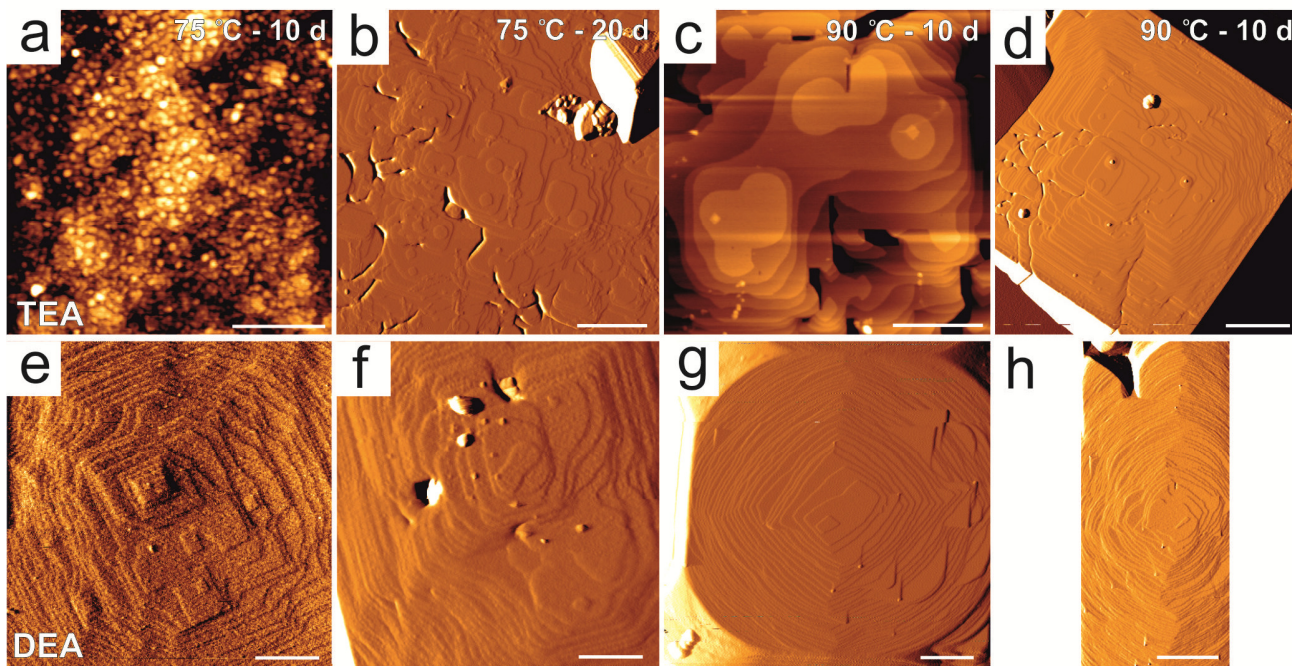


**Figure 3.** AFM height and deflection images from Batch 1 experiments. a-d) Experiments performed with TEA at 75 °C-10 days (a), 75 °C- 20 days (b) and 90 °C – 10 days (c - d). e- h) Experiments performed with DEA at 75 °C-10 days (e), 75 °C- 20 days (f) and 90 °C – 10 days, {100} face (g) {110} (h). Scale bars: a, e, f, g = 0.5  $\mu\text{m}$ ; b, c, h = 1  $\mu\text{m}$ ; d, 2  $\mu\text{m}$ .

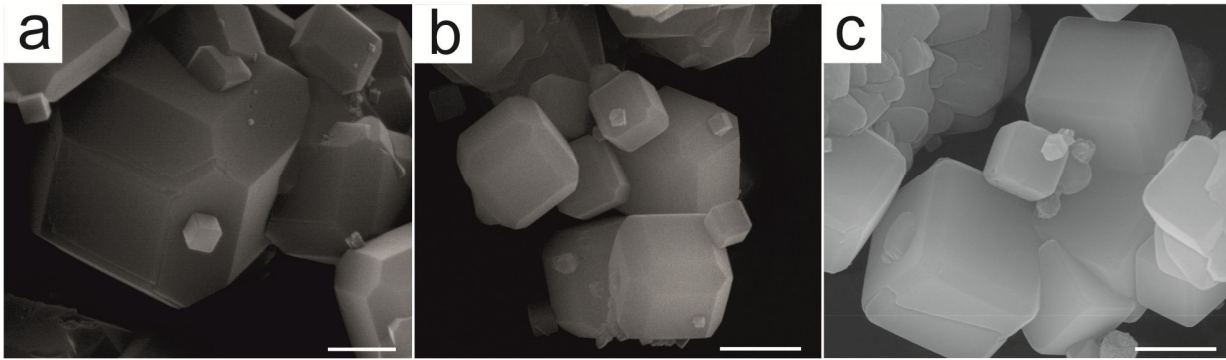


**Figure 4.** SEM micrographs from selected experiments from batch 2. a) 60 °C – 12 days, b) 75 °C – 7 days and c) 90 °C – 4 days. Scale bars: a = 2  $\mu\text{m}$ ; b, c = 5  $\mu\text{m}$ .

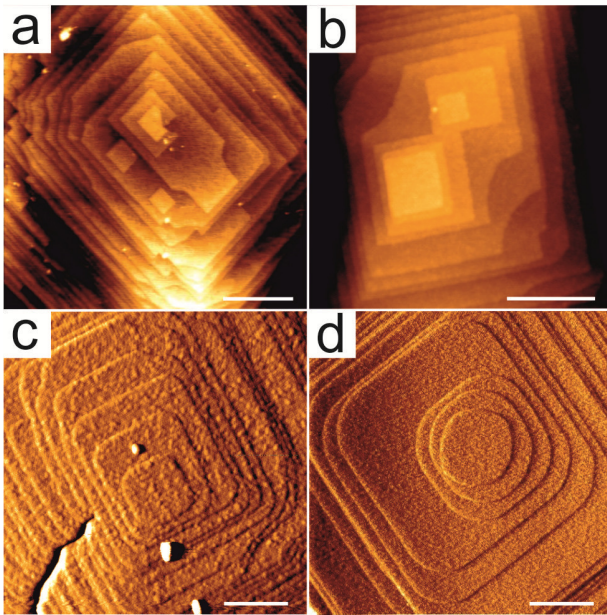


**Figure 5.** AFM height and deflection images from selected experiments from Batch 2. a) 60 °C – 14 days, b) 75 °C – 10 days, c) 90 °C – 2 days, 90 °C – 10 days. Scale bars: 5  $\mu\text{m}$ .

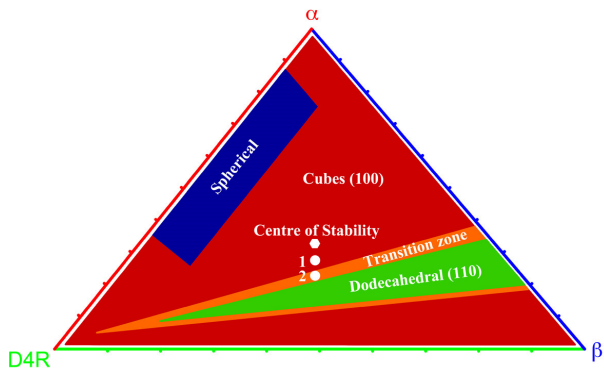


**Figure 6.** Triangular plot showing the basic crystal habit of LTA crystals depending on the relative energy penalties of the three cage types: D4R; BETA; ALPHA. For example, at the apex labelled D4R the relative energy penalties would be D4R:BETA:ALPHA = 1:0:0. At the Centre of Stability the relative energy penalties would be D4R:BETA:ALPHA = 0.33:0.33:0.33.

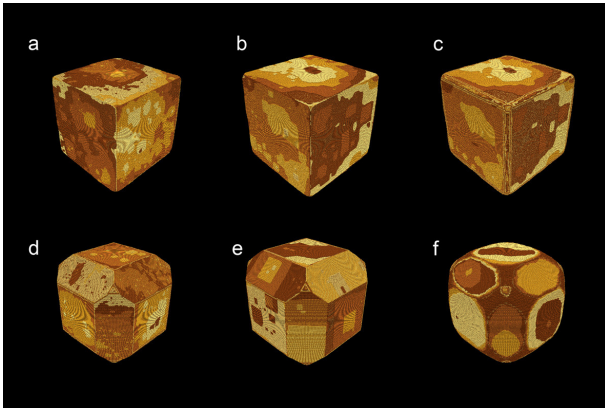


**Figure 7.** Simulations of crystal morphology and surface topology of LTA crystals grown with the energy penalties of cages at positions 1 (a, b and c) and 2 (d, e and f) on Figure 6. Supersaturated (a and d), equilibrium (b and e), undersaturated (c and f).

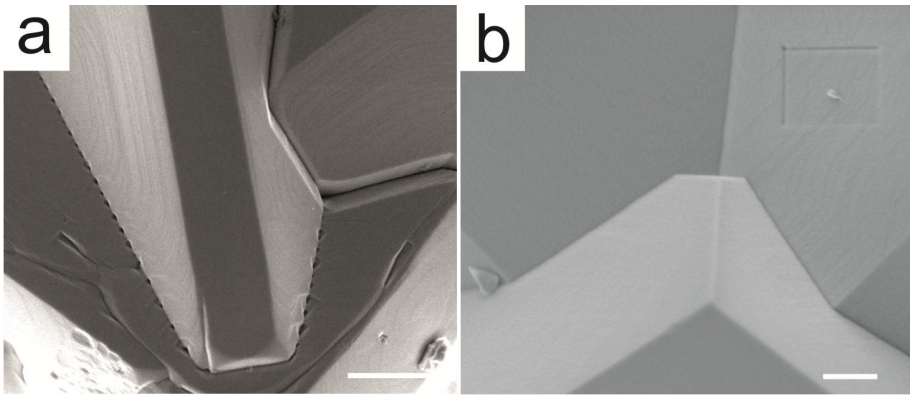


**Figure 8.** High-resolution SEM images showing triangular etch pits (a) along the twin boundary of crystals grown at 90 °C as a result of undersaturation caused by successive crystal transformation. The phenomenon is not present at the lower temperature (75 °C) (b). Scale bars: a = 1  $\mu\text{m}$ ; b = 200 nm.

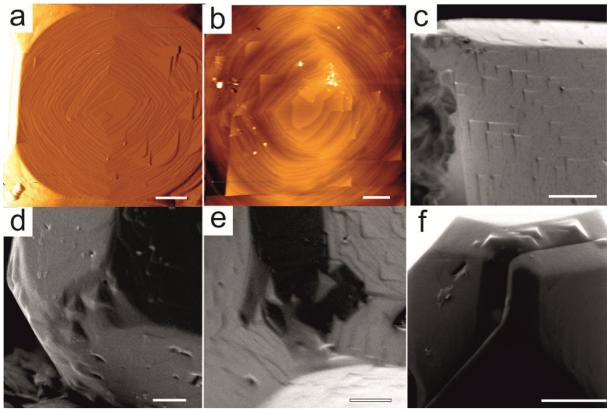


**Figure 9.** High-resolution SEM images of zeolite A undergoing successive crystal transformation at undersaturated conditions. Terrace retreat exposes point defects which serve to pin the retreat and result in rectilinear surface protusions. Scale bars: a, b, f = 500 nm; c, d, e = 200 nm.

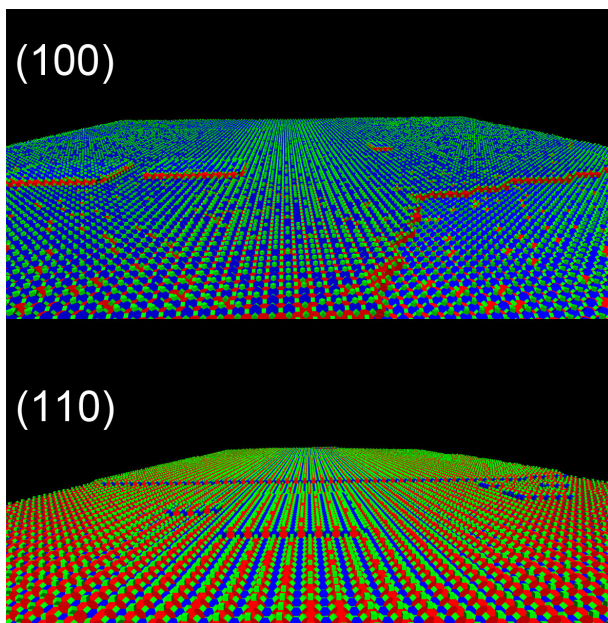


**Figure 10.** Simulated surface structures for simulation corresponding to position 2 in Figure 6 determined at equilibrium for the (100) and (110) faces of LTA. The cages are colour coded: green for D4R; blue for BETA cage; red for ALPHA cage.

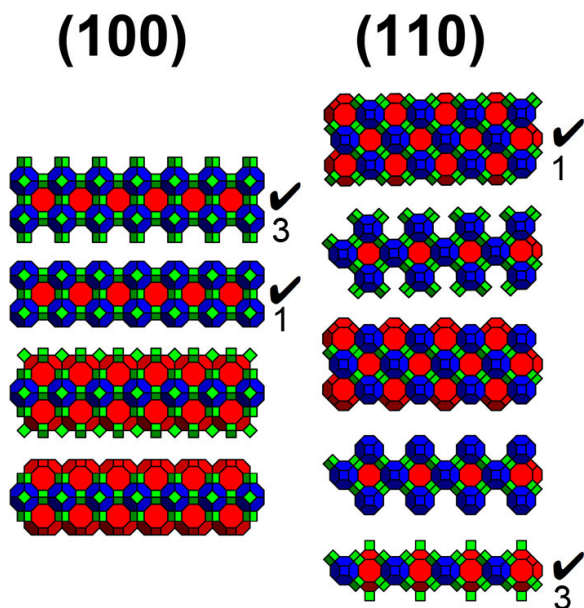


**Figure 11.** Possible surface termination structures for the LTA structure based upon closed cages. The cages are colour coded: green for D4R; blue for BETA cage; red for ALPHA cage. The structures found are indicated with a tick along with the relative concentration of the structures for equilibrium simulations based upon position 2 in Figure 6.

**TOC Graphic**

